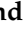# Non-Invasive Physical Plasma Enhances the Membrane Permeability to Low Molecular Weight Compounds and Subsequently Leads to the Loss of Cellular ATP and the Devitalization of Epithelial Cancer Cells

Caroline Sander [1], Andreas Nitsch [1], Holger H. H. Erb [2,3], Eva K. Egger [4], Lyubomir Haralambiev [1], Benedikt Eggers [5], Franz-Josef Kramer [5], Martin Weiss [6], Alexander Mustea [4] and Matthias B. Stope [3,4,*]

[1] Department of Trauma, Reconstructive Surgery and Rehabilitation Medicine, University Medicine Greifswald, Ferdinand-Sauerbruch-Straße, 17475 Greifswald, Germany; cs166368@uni-greifswald.de (C.S.); an124100@uni-greifswald.de (A.N.); lyubomir.haralambiev@uni-greifswald.de (L.H.)

[2] Department of Urology, Technische Universität Dresden, Fetscherstraße 74, 01307 Dresden, Germany; holger.erb@uniklinikum-dresden.de

[3] UroFors Consortium (Natural Scientists in Urological Research) of the German Society of Urology, Uerdinger Straße 64, 40474 Düsseldorf, Germany

[4] Department of Gynecology and Gynecological Oncology, University Hospital Bonn, Venusberg-Campus 1, 53127 Bonn, Germany; eva-katharina.egger@ukbonn.de (E.K.E.); alexander.mustea@ukbonn.de (A.M.)

[5] Department of Oral & Maxillofacial Plastic Surgery, Center of Dento-Maxillo-Facial Medicine, University Hospital Bonn, Welschnonnenstraße 17, 53111 Bonn, Germany; benedikt.eggers@ukbonn.de (B.E.); franz-josef.kramer@ukbonn.de (F.-J.K.)

[6] Department of Women's Health Tübingen, Eberhard-Karls-University Tübingen, Calwerstraße 7, 72076 Tübingen, Germany; martin.weiss@med.uni-tuebingen.de

*   Correspondence: matthias.stope@ukbonn.de; Tel.: +49-228-287-11361

Abstract: Non-invasive physical plasma (NIPP) achieves biomedical effects primarily through the formation of reactive oxygen and nitrogen species. In clinical use, these species interact with cells of the treated tissue, affecting the cytoplasmic membrane first. The present study investigated the permeability of the cytoplasmic membrane of breast cancer cells with different fluorescent dyes after NIPP treatment and determined the subsequent effects on cell viability. After NIPP treatment and the associated formation of reactive oxygen species, low molecular weight compounds were able to pass through the cytoplasmic membrane in both directions to a higher extent. Consequently, a loss of cellular ATP into the extracellular space was induced. Due to these limitations in cell physiology, apoptosis was induced in the cancer cells and the entire cell population exhibited decreased cell growth. It can be concluded that NIPP treatment disturbs the biochemical functionality of the cytoplasmic membrane of cancer cells, which massively impairs their viability. This observation opens a vast application horizon of NIPP therapy to treat precancerous and malignant diseases beyond breast cancer therapy.

Keywords: physical plasma; non-invasive; mamma carcinoma; breast cancer; cytoplasmic membrane; chemo-sensitivity

1. Introduction

Physical plasma is the fourth state of matter and corresponds to a highly energized, partially or fully ionized gas [1]. Medical physical plasma, which only reaches temperatures slightly above human body temperature, is also used in therapy. The biomedical effects include antiseptic, anti-inflammatory, and antimicrobial activity on tissues, which has been used in dermatological treatments [2,3]. A comparatively new field of application is plasma oncology. Here, devitalizing effects combined with simultaneous preservation of the surrounding tissue are used to treat solid tumors. This non-invasive physical plasma

(NIPP) primarily exerts its activity via reactive oxygen and nitrogen species formed at the interface between NIPP and the ambient atmosphere. These reactive species exhibit antiproliferative, antimetastatic, and proapoptotic effects on cells and tissues [4,5].

Therefore, NIPP treatment provides potent antioncogenic efficacy and a new treatment strategy. The antioncogenic effects were observed in different in vitro models, including skeletal sarcoma, ovarian, prostate, pancreatic, and lung cancer cell models [6–10].

The cytoplasmic membrane partitions intracellular and extracellular reaction spaces of eukaryotic cells and is the first to be affected by exogenous chemical and physical noxae. The maintenance of osmotic and electrochemical gradients at the cytoplasmic membrane is essential for cell physiology and is maintained by the protein and lipid components of the membrane [11]. While small nonpolar molecules can pass through the cytoplasmic membrane almost unhindered, there are passive and active transport systems for larger and charged molecules, some of which are energy dependent. These are regulated in a complex manner and are crucial for cell physiology [12]. Due to the formation of reactive species, a NIPP impact on the biochemical integrity and functionality of the cytoplasmic membrane is reasonably likely. Recent studies in this field have indicated protein and lipid oxidations by NIPP [13,14].

This study aimed to characterize the permeability of the cytoplasmic membrane after NIPP treatment. For this purpose, the passability of low molecular weight compounds through the cytoplasmic membrane and the effects on cellular viability resulting from NIPP treatment were investigated. Regarding a potential NIPP application in plasma oncology, breast cancer was selected as a cellular model. Worldwide, breast cancer is one of the most common cancers and one of the leading causes of cancer-associated death in women [15]. Current treatment options include surgical resection, chemotherapy, endocrine therapy, immunotherapy, and radiation therapy. In many cases, a combination of treatment options is inevitable, leading to increased toxicity [16]. Therefore, NIPP treatment, which has minimal side effects, appears to be a promising alternative for improving therapeutic options in breast cancer treatment.

2. Materials and Methods

2.1. Cell Culture

Human breast cancer cell lines MCF-7 and MDA-MB-231 (American Type Culture Collection, Manassas, VA, USA) were propagated in Dulbecco's Modified Eagle Medium (DMEM)/F12 containing 10% fetal bovine serum (FBS) and 0.125% gentamicin (all from PAN Biotech, Aidenbach, Germany). Cells were incubated in humidified atmosphere at 5% CO_2 and 37 °C and passaged twice a week.

2.2. Non-Invasive Physical Plasma Treatment

A medical argon plasma jet device was used to treat cells with non-invasive physical plasma (NIPP) (Kinpen Med, Neoplas Tools, Greifswald, Germany) (Figure 1). The device generates a NIPP flame approximately 1 cm long at the tip of the handpiece. The carrier gas argon was set to a flow rate of 4.0 L/min. The plasma jet device is designed for manual operation. For the majority of the assays performed, NIPP treatment was performed in 24-well cell culture plates. Therefore, cells were diluted in 200 µL of medium or Dulbecco's phosphate-buffered saline (DPBS, PAN Biotech). To treat the cancer cells, the NIPP flame was applied over the surface of the liquid in a continuous bidirectional motion so that the tip of the NIPP flame touched the medium of the cell suspension. The distance from the tip of the handpiece to the surface of the cell culture medium was approximately 1.0 cm. After treatment, the cell suspension was transferred to a new cell culture plate.

For microscopic analyses, cells were seeded on coverslips and incubated for 24 h. Treatment was then performed with coverslips overlaid with DPBS to prevent the cells from drying out. For this purpose, the NIPP flame was moved uniformly over the coverslip in a meandering motion. Argon treatments in which the NIPP flame was not ignited served as controls.

Figure 1. The Kinpen Med medical argon plasma device (Neoplas Tools, Greifswald, Germany) was used to generate non-invasive physical plasma (NIPP).

2.3. Temperature Measurement on Liquids

Two different measuring devices were used to determine the cell culture medium temperature during NIPP treatment. The detection of the surface temperature of the liquid was performed by a FLIR One infrared camera (Teledyne Flir, Wilsonville, OR, USA). The temperature below the liquid surface was determined using a Lab Thermometer IP65 with an LT-101 temperature sensor (TFA Dostmann, Reicholzheim, Germany).

2.4. Detection of Plasma Ignition at Different Carrier Gas Flow Rates

To investigate the influence of the carrier gas flow rate on the ignition of the plasma flame, different flow rates from 1.0 to 6.5 L/min were set on the device and the device was started. The ignition of the plasma flame was documented by means of photography.

2.5. Hydrogen Peroxide (H_2O_2) Assay

The formation of H_2O_2 after NIPP treatment was verified by applying a Molecular Probes Amplex Red Hydrogen Peroxide/Peroxidase Assay Kit (Thermo Fisher Scientific, Waltham, MA, USA). For this purpose, 200 μL of ultrapure water was treated with NIPP for 5, 10, 20, 40, and 80 s. Each examination was performed with 4.0, 4.5, and 5.0 L/min gas flow. The following treatment was analogous to the treatment in the other experiments. NIPP-treated ultrapure water was diluted at 1:100 and the assay was carried out according to the manufacturer's instructions. The data were analyzed using a two-way ANOVA. Multiple Tukey comparisons were made. In addition, regression analyses were carried out.

2.6. Microscopic Dextran-Fluorescein Isothiocyanate (FITC) Uptake Assay

Breast cancer cells were seeded on 24×40 mm coverslips (Paul Marienfeld, Laude-Königshofen, Germany) and incubated for 24 h in DMEM/F12 medium. To ensure complete medium removal, the coverslips were washed five times in DBPS and transferred to 2 mL of fresh DPBS. Subsequently, cells were treated with NIPP for 20 and 60 s and incubated with 10 μL of dextran-fluorescein isothiocyanate (FITC, 30 mg/mL; Sigma-Aldrich, St. Louis, MO, USA) and 100 μL of 4′ 6-diamidino-2-phenylindole (DAPI, 1 μg/mL; Carl Roth, Karlsruhe, Germany) for 2 min. After being washed five times in DPBS, the stained cells were analyzed by fluorescence microscopy using DAPI and green fluorescent protein (GFP) channels with a BZ-9000 microscope with BZ-II Analyzer software (Keyence Corporation, Osaka, Japan). For analysis, the FITC-positive area was determined and correlated to the number of DAPI-positive nuclei (FITC signal/cell).

2.7. Fluorescein Release Assay

Cells were suspended by trypsin/ethylenediaminetetraacetic acid (EDTA) treatment, stopped by DPBS containing 10% FBS (stop solution), and sedimented ($300 \times g$, 5 min). Cells

were immediately diluted in DPBS (1,000,000 cells/mL) and treated with NIPP for 20 and 60 s. This procedure was followed by transferring 200 µL cell suspension to a cytometry tube and the loading of cells with fluorescein diactetate (FDA) and ethidium bromide (200 µL loading solution containing 60 µg/mL ethidium bromide and 10 µg/mL FDA in DPBS) for 15 min on ice in the dark. Cells were then diluted in 2 mL of DPBS, sedimented ($300 \times g$, 5 min, 4 °C), and resuspended in 300 µL of DPBS. The dye-loaded cells were then analyzed using a BD FACSCanto™ flow cytometer (BD Biosciences, Heidelberg, Germany) with FACSDiva™ 6.0 software (BD Biosciences). Based on forward- and side-scatter, gating strategies were used to exclude dead cells, cell debris, and doublets (Figure 2). FlowJo software version 10 (Tree Star Inc., Ashland, OR, USA) was used for analysis. Mean fluorescence intensity was calculated, and the values of the NIPP-treated cells were normalized to argon-treated control cells (control = 1.0).
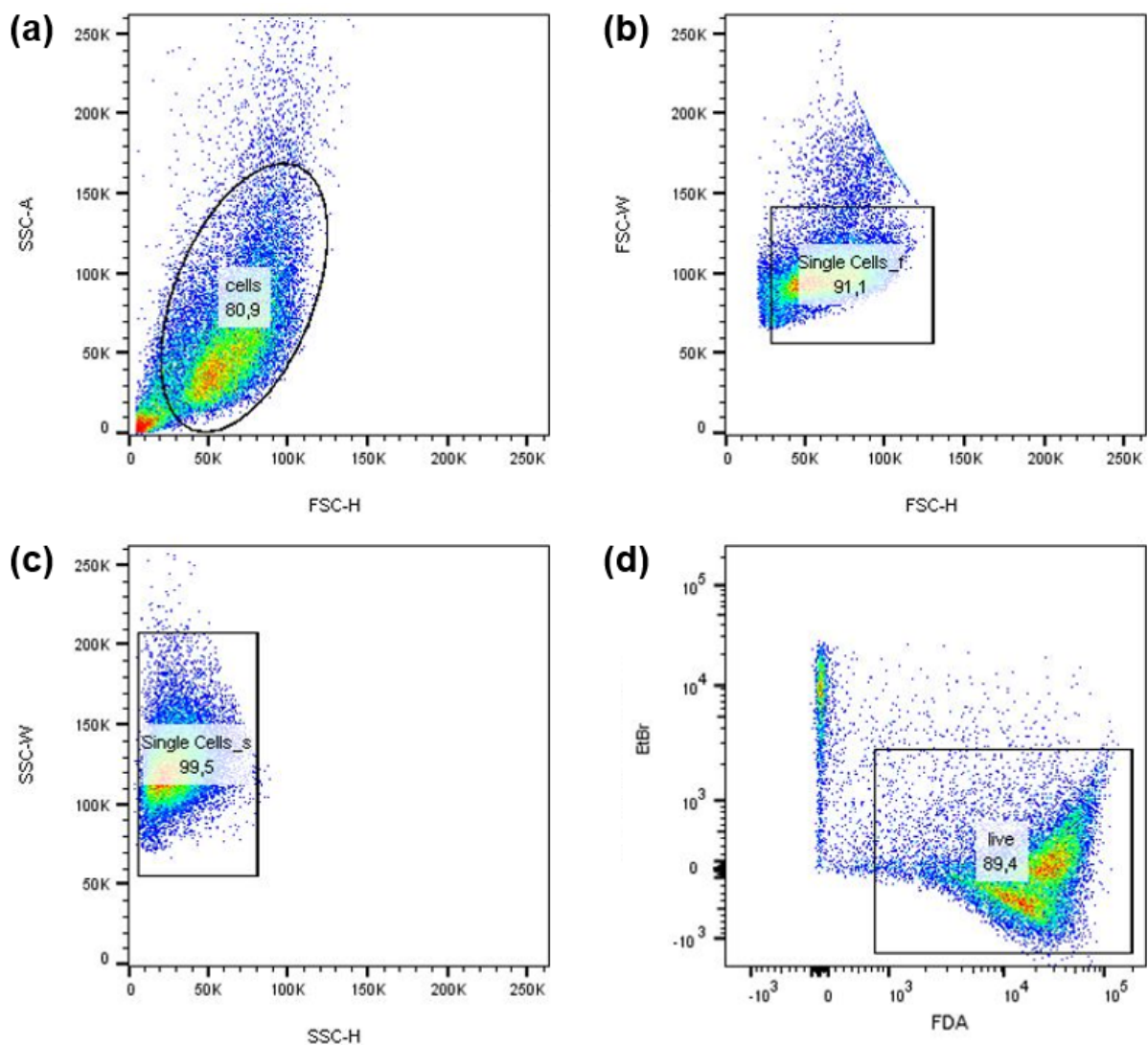
Figure 2. Gating strategy in flow cytometric analyses. The intracellular content of fluorescein-diacetate (FDA) per cell was examined by flow cytometry. Using forward- and side-scatter-parameters, debris (**a**) and doublets (**b,c**) were rejected. Living cells were determined as ethidium bromide (EtBr) negative and FDA positive events (**d**). Abbreviations: side-scatter area, SSC-A; forward-scatter width, FSC-W; forward-scatter height, FSC-H; side-scatter width, SSC-W; side-scatter height, SSC-H.

2.8. ATP Release Assay

Cells were separated by trypsin/EDTA treatment, mixed with stop solution (10% FBS in DPBS), and sedimented ($300\times g$, 5 min). Subsequently, 1,000,000 cells/mL were diluted in DPBS and 200 μL of this cell suspension was treated with NIPP for 20, 60, and 120 s. Treated cells were incubated for 10 min at room temperature, sedimented ($3000\times g$, 5 min), and 100 μL of the cell-free supernatant was transferred to a 96-well microtiter plate. Then, 100 μL of CellTiter-Glo 2.0 ATP reagent (Promega, Walldorf, Germany) was added to each preparation. Subsequently, luminescence was detected in an infinite M200 Pro microplate reader (Tecan, Männedorf, Switzerland). The values of the NIPP-treated cells were normalized to argon-treated control cells (control = 1.0).

2.9. Caspase-3/7 (Casp-3/7) Apoptose Assay

To analyze caspase-3 and -7 activity after NIPP treatment, 20,000 (72 h incubation), 40,000 (48 h incubation), and 80,000 (24 h incubation) MCF-7 cells and 15,000 (72 h incubation), 30,000 (48 h incubation), and 60,000 (24 h incubation) MDA-MB-231 cells were treated for 20 s with NIPP and incubated in a 96-well cell culture plate for 24, 48, and 72 h at 37 °C and 5% CO_2. Cells were sedimented ($1000\times$ g, 3 min), the cell culture medium was discarded, and the cells were incubated (37 °C, 45 min) with 100 μL of caspase-3/7 detection solution (5 μM CellEvent™ Caspase-3/7 Green Detection Reagent (Thermo Fischer Scientific) in DPBS containing Ca^{2+} and Mg^{2+} (PAN Biotech) with 5% FBS). Fluorescence excitation was performed at 495 nm and emission was measured at a maximum of 535 nm in the Infinite M200 Pro microplate reader (Tecan). At the same time, a cell culture plate was included for determining the number of viable cells with a CASY Cell Counter and Analyzer model TT (Roche Applied Science, Mannheim, Germany) to normalize the fluorescence intensity to the number of cells. The values of the NIPP-treated cells were normalized to argon-treated control cells (control = 1.0). Samples lacking the detection reagent (negative control) and samples treated with staurosporine instead of NIPP (positive control) were included as controls.

2.10. Terminal Deoxynucleotidyl Transferase dUTP Nick End Labeling Apoptose Assay

Twenty thousand (72 h incubation), 40,000 (48 h incubation), and 80,000 (24 h incubation) MCF-7 cells and 15,000 (72 h incubation), 30,000 (48 h incubation), and 60,000 (24 h incubation) MDA-MB-231 cells were treated with NIPP for 20 s and then incubated in 96-well scale for 24, 48, and 72 h at 37 °C and 5% CO_2. According to the manufacturer's instructions, the TiterTACS in situ apoptosis detection kit (Trevigen, Gaithersburg, MD, USA) was used to determine DNA double-strand breaks induced by apoptosis. Absorbance at 630 nm was measured every minute in the Infinite M200 Pro microplate reader (Tecan). When the linear range was left, the reaction was stopped by adding 100 μL of 0.2 M hydrochloric acid (Merck, Darmstadt, Germany) and an absorbance measurement (450 nm) was performed. The signal intensity of the 450 nm absorbance was normalized to the cell number. For this purpose, a parallel cell culture plate was prepared and the number of cells in each sample was examined. Values of NIPP-treated cells were normalized to argon-treated control cells (control = 1.0). Samples without the transferase enzyme (negative control) and samples with DNA nuclease (positive control) were included as controls.

2.11. mRNA Analysis of the Pro-Apoptotic Regulators: Bcl-2 Antagonist of Cell Death (BAD) and Caspase-9 (Casp-9)

One hundred thousand (MCF-7) and 70,000 (MDA-MB-231) cells were treated with NIPP for 20, 60, and 120 s and then incubated in a 24-well plate for 48 h at 37 °C and 5% CO_2. Total RNA was prepared (RNA Extraction Kit, Qiagen, Hilden, Germany) and reverse transcribed (RT) into cDNA using an iScript Select cDNA Synthesis Kit (Bio-Rad Laboratories, Munich, Germany). cDNA in the amount of 1.0 μL was used as a template in the polymerase chain reaction (PCR; SsoAdvanced Universal SYBR Green Supermix, Bio-Rad Laboratories, with BAD and Casp-9-specific commercial primers, QuantiTect

Primer Assay, Qiagen). The PCR protocol included initial denaturation (95 °C, 5 min) and 40 cycles of denaturation (95 °C, 10 s) and combined annealing/elongation (60 °C, 30 s). The mRNA expression of BAD and CASP9 was detected in an iCycler iQ5™ system (Bio-Rad Laboratories) and evaluated by the comparative threshold cycling method. The reference gene was glyceraldehyde-3-phosphate dehydrogenase (GAPDH).

2.12. Cell Growth Assay

For the cell growth assay, 45,000 (MCF-7) and 30,000 (MDA-MB-231) cells were treated with NIPP for 20 s, and the treated cells were incubated for 24, 48, 72, 96, and 120 h at 37 °C and 5% CO_2. Cell growth was monitored using a CASY Cell Counter and Analyzer model TT (Roche Applied Science). Cells were treated with trypsin/EDTA (PAN Biotech), suspended, and then diluted in 10 mL of CASYton (Roche Applied Science). For cell counting, 3×400 μL of this dilution was measured. Cell-specific gate settings of 7.60 μm/14.55 μm (MCF-7) and 6.90 μm/12 μm (MDA-MB-231) were used to differentiate live cells, dead cells, and cellular debris.

2.13. Statistics

Graph Pad Prism V 5.01 (GraphPad Software, La Jolla, CA, USA) graphics and statistical software was used for data analysis and presentation of results. Unless otherwise stated in the method description, statistical analyses were performed using Student's *t*-test and significances were defined as follows: $p \leq 0.05$ (*), $p \leq 0.01$ (**), $p \leq 0.001$ (***).

3. Results

In the medical application of NIPP, no thermal effects occur on the tissue, but reactive oxygen species (ROS) are formed. These highly reactive molecules are the most important active components in oncological NIPP therapy [5]. According to their biochemical properties, ROS can oxidize biomolecules and impair their molecular and cellular functionality. As the outermost layer of eukaryotic cells, the lipid and protein components of the cytoplasmic membrane are particularly affected, which might have consequences for the directional and fine-tuned permeability characteristics of the membrane [17,18].

3.1. Basic Characterization of the NIPP Action in an In Vitro Cancer Cell Model

The specific biological effect of NIPP is based on the principle that a cold physical plasma is being generated and no thermal effects are affecting the cells [1]. The measurement of the surface temperature (Figure 3a) and the immersion temperature (Figure 3b) of the cell culture medium at room temperature even showed a slight temperature decrease during 120 s of NIPP treatment. Heat stress or thermal damage could therefore be excluded within the treatment durations used.

The physicochemical and thus biomedical properties of NIPP depend on the flow rate of the carrier gas. However, the possibilities for variation are limited with the device used, since the NIPP effluent only ignites in a flow rate range of 4.0–5.5 L/min (Figure 3c). To reduce the mechanical stress during treatment, all the following experiments were therefore carried out with the lowest possible flow rate of 4.0 L/min.

Examinations of H_2O_2 formation during NIPP treatment demonstrated that the formation rate depended predominantly on the treatment duration and only slightly on the flow rate (Figure 3d). The concentration of H_2O_2 depended on the flow rate of the carrier gas and on the treatment duration (F (16, 50) = 3.248; $p < 0.001$). A higher flow rate of the carrier gas and a longer treatment duration led to higher H_2O_2 concentrations. Multiple comparisons showed that significant differences depending on the flow rate appeared only after longer treatment durations. No significant difference could be detected after 5, 10, and 20 s of NIPP treatment. After a treatment time of 40 s, the flow rates of 5.0 L/min differed significantly ($p = 0.005$). The flow rate had a significant effect on the H_2O_2 formation only at a treatment duration of 80 s (4.0 L/min vs. 5.0: $p = 0.006$). Further analyses showed that the concentration of H_2O_2 was linearly related to the treatment time ($r^2 = 0.977$). No linear

relationship could be demonstrated as a function of the flow rate. Thus, variable treatment durations and a constant flow rate was used for further investigations.
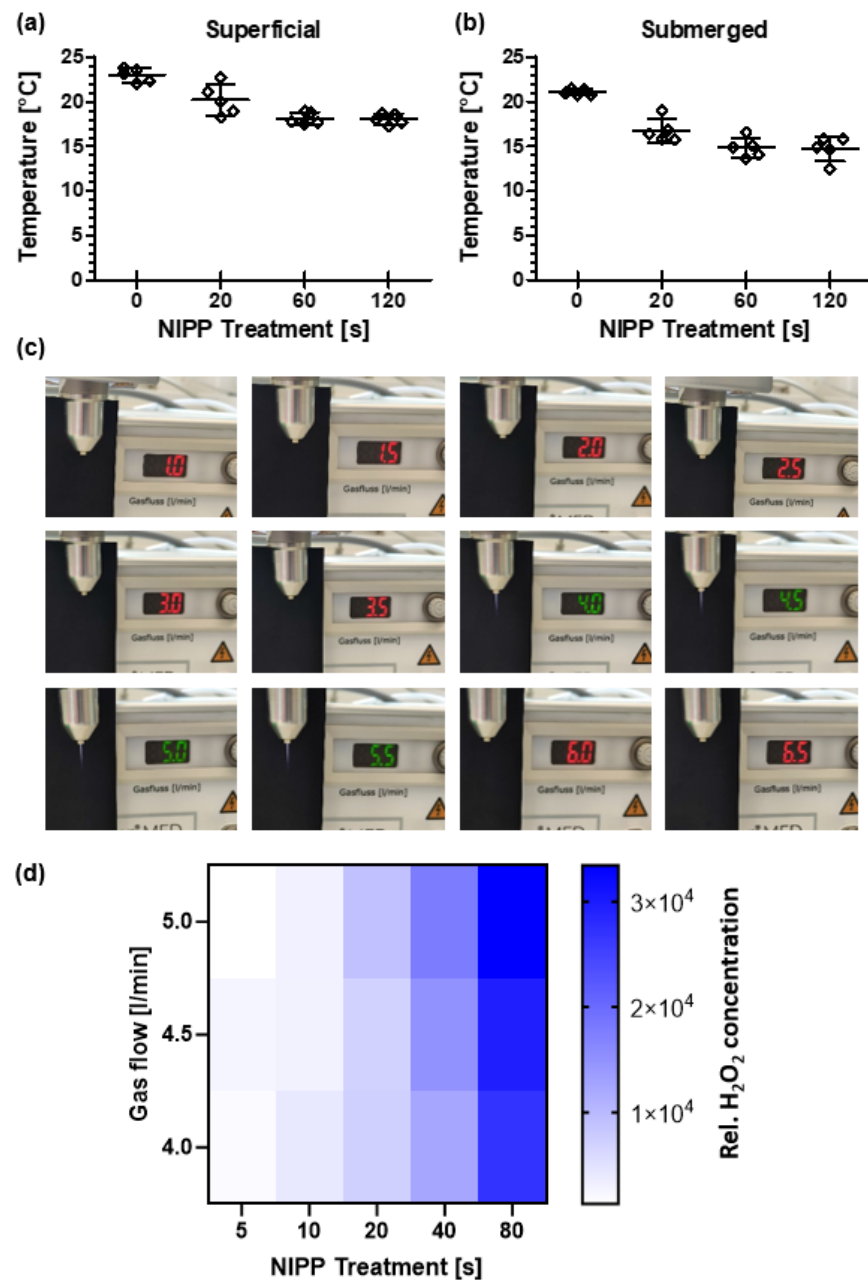

Figure 3. Basic NIPP characterization. (**a**) Superficial (FLIR One infrared camera, Teledyne Flir) and (**b**) submerged (Lab Thermometer IP65 with an LT-101 temperature sensor, TFA Dostmann) temperature variations of cell culture medium at room temperature during 120 s of NIPP treatment. (**c**) Flame pattern after ignition of the NIPP flame at carrier gas flow rates from 1.0 to 6.5 L/min. The flow rates are shown in the device's own display. (**d**) H_2O_2 formation after NIPP treatment. Ultrapure water was treated with NIPP at flow rates of 4.0, 4.5, and 5.0 L/min and treatment durations of 5 to 80 s. The relative H_2O_2 concentrations were determined by a Molecular Probes Amplex Red Hydrogen Peroxide/Peroxidase Assay Kit (Thermo Fisher Scientific).

3.2. NIPP Affects the Cytoplasmic Membrane of Cancer Cells and Causes the Influx of FITC-Labeled Dextran

To evaluate if NIPP exposure increased the cytoplasmic membrane permeability to low molecular weight compounds, breast cancer cells were incubated with FITC-labeled

10 kDa dextran after 20 and 60 s of NIPP treatment. Microscopic analysis of the intracellular FITC signal revealed that significantly higher amounts of dextran-FITC penetrated the cells after both NIPP treatment durations (Figure 4a,c). This effect was observed for both cancer cell lines, MCF-7 and MDA-MB-231, although no dependence on NIPP exposure time was observed (Figure 4b,d).
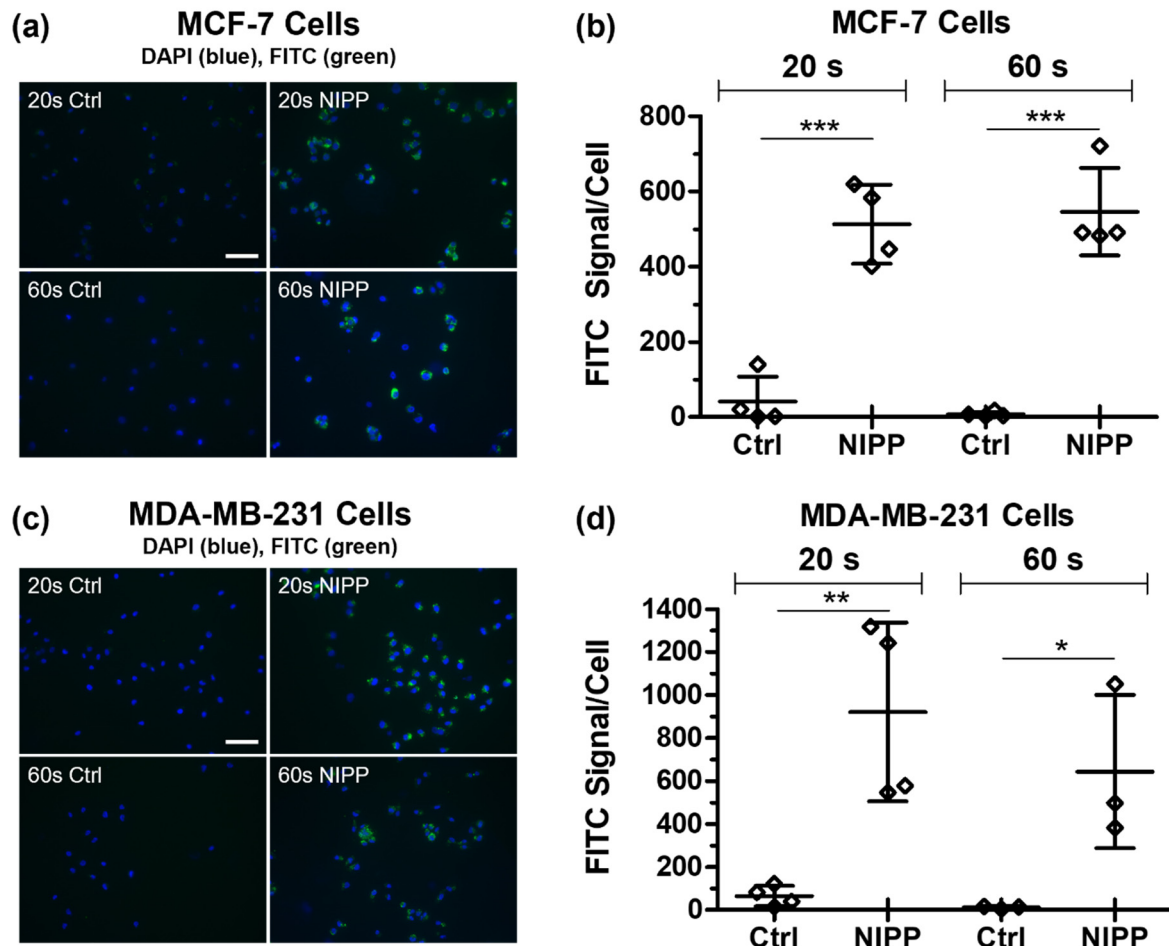

Figure 4. Microscopic dextran-fluorescein isothiocyanate (FITC) uptake assay. Breast cancer cells MCF-7 (**a,b**) and MDA-MB-231 (**c,d**) were seeded on coverslips, treated with NIPP for 20 and 60 s, and stained with 10 μL of dextran-FITC and 100 μL DAPI for 2 min. Cells were analyzed by fluorescence microscopy (BZ-9000 microscope with BZ-II analyzer software, scale bars represent 50 μm). For analysis, the FITC-positive area was determined and correlated to the number of DAPI-positive nuclei (FITC signal/cell). The results are displayed as mean $\pm$ standard deviation ($p \leq 0.05$ *; $p \leq 0.01$ **; $p \leq 0.001$ ***).

3.3. NIPP-Induced Alteration of the Cytoplasmic Membrane Enables the Efflux of Non-Membrane-Permeable Fluorescein

In the following, data were confirmed using an alternative technique. NIPP-treated cells were loaded with fluorescein diacetate (FDA), washed, and subsequently analyzed by flow cytometry. FDA is particularly suitable for such studies because the lipophilic FDA is converted intracellularly by cellular esterases to the hydrophilic, membrane-impermeable dye fluorescein, which accumulates in the cell [19].

Flow cytometric evaluation of the FDA-loaded cells showed that they released the fluorescent dye significantly after NIPP treatment in comparison to argon-treated control cells (Figure 5). Although the enzymatic cleavage of FDA to fluorescein should have prevented the dye from bleeding out of the cells, the dye accumulated significantly less in the breast cancer cells after 20 and 60 s of NIPP treatment. Again, the NIPP exposure time did not seem to affect the strength of the effect.
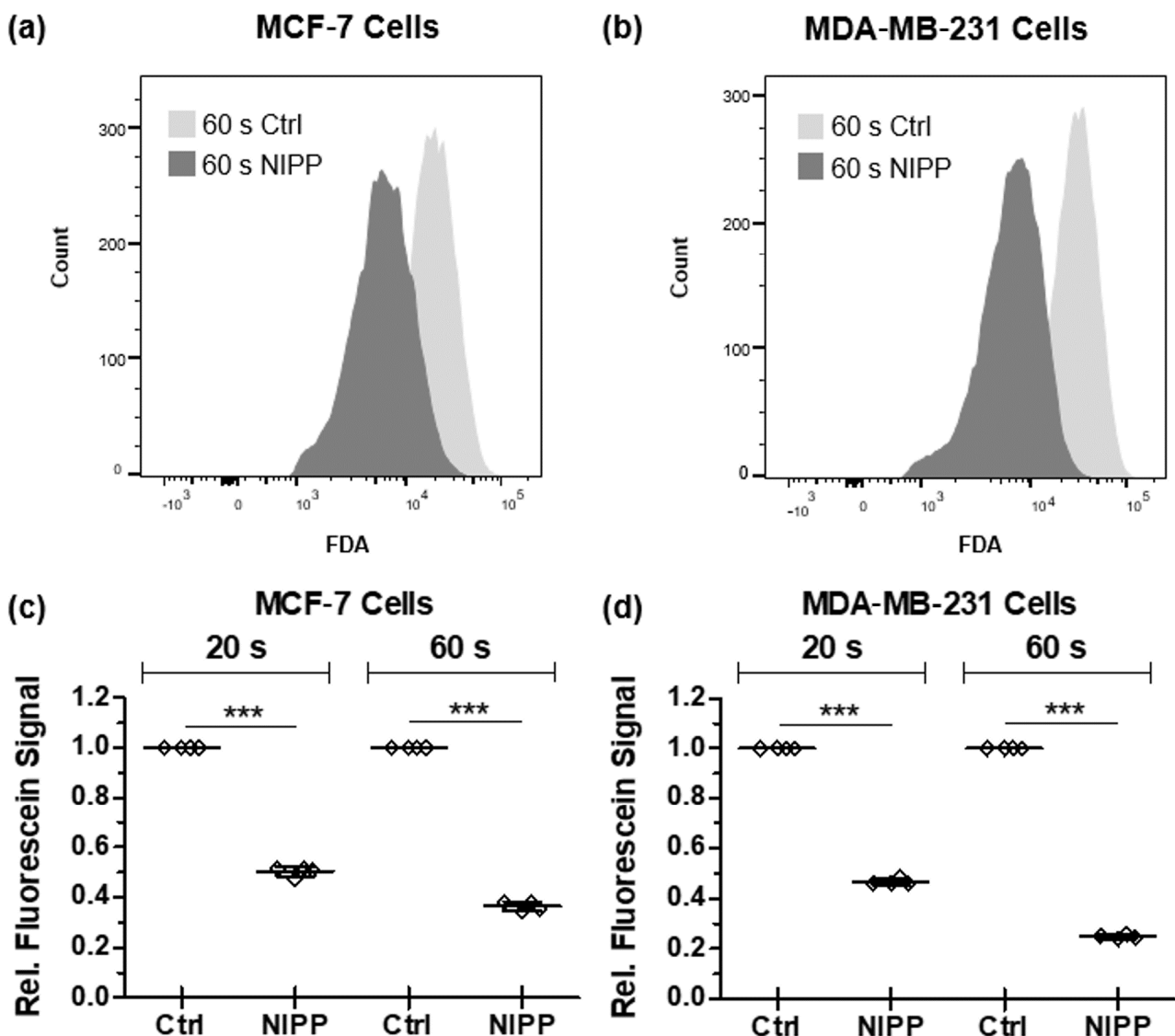
Figure 5. Fluorescein release assay. Breast cancer cells MCF-7 (**a**,**c**) and MDA-MB-231 (**b**,**d**) were treated with NIPP for 20 and 60 s, and loaded with membrane-permeable fluorescein diacetate (FDA). (**a**,**b**) Flow cytometric raw data of 60 s of NIPP treatment. Control cells were treated with argon for appropriate times (Ctrl). The enzymatic conversion of FDA to non-membrane permeable fluorescein prevents the release of the dye under physiological conditions. Fluorescein release was determined by flow cytometry (BD FACSCanto™ flow cytometer and FlowJo software version 10) and expressed as relative signal normalized to controls. The results are displayed as mean $\pm$ standard deviation ($p \leq 0.001$ ***).

3.4. NIPP-Induced Alteration of the Cytoplasmic Membrane Enables the Efflux of Endogenous ATP Molecules

Finally, altered cytoplasmic membrane permeability after NIPP treatment was examined in a third approach. ATP is a central biomolecule in metabolism and is not released from cells under normal physiological conditions.

Therefore, ATP release was determined after NIPP exposure to measure changes in membrane permeability without nonphysiological or potentially toxic dye incubation. Furthermore, the duration of NIPP treatment was additionally extended to 120 s to demonstrate the suggested dependence between dosage and cellular effect. It was shown that NIPP-treated MCF-7 cells released significantly more ATP into the cell culture supernatant after 60 and 120 s of NIPP treatment than was detectable in the control approaches (Figure 6a). However, a 20 s treatment duration demonstrated only a tendential but not statistically significant extracellular ATP increase. In NIPP-treated MDA-MB-231 cells, significantly

elevated extracellular ATP concentrations were measurable after 20, 60, and 120 s of NIPP treatment (Figure 6b). For the NIPP-induced ATP release, the effect increased with a more extended treatment duration.
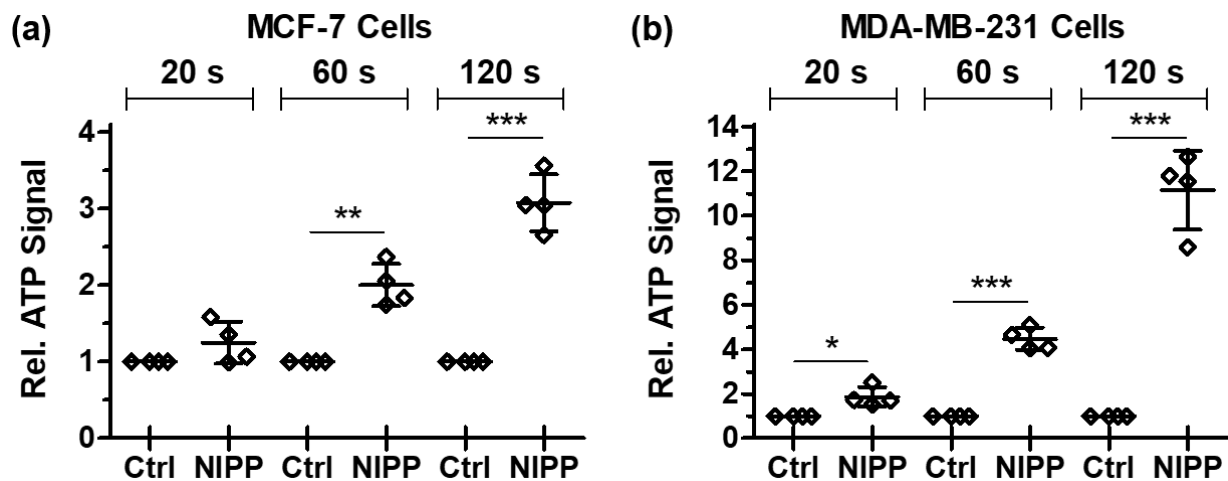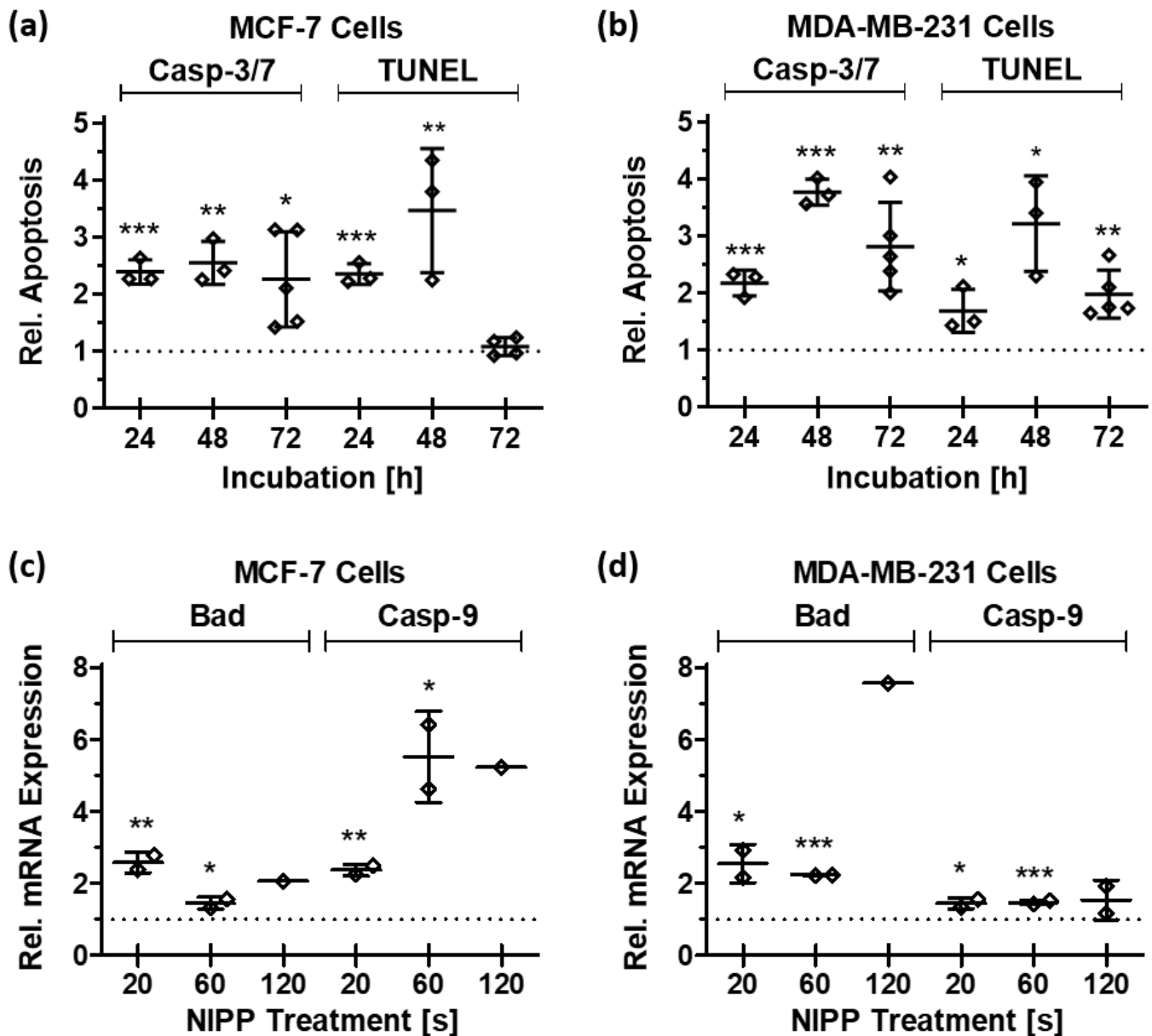

Figure 6. ATP release assay. Breast cancer cells MCF-7 (**a**) and MDA-MB-231 (**b**) were treated with non-invasive physical plasma (NIPP) for 20, 60, and 120 s and incubated for 10 min at room temperature. Control cells were treated with argon for appropriate times (Ctrl). Subsequently, cell-free supernatant was measured with CellTiter Glo 2.0 ATP reagent (infinite M200 Pro microplate reader) to determine extracellular ATP. ATP concentrations were expressed as relative signal normalized to controls. The results are displayed as mean ± standard deviation ($p \leq 0.05$ *; $p \leq 0.01$ **; $p \leq 0.001$ ***).

3.5. NIPP Treatment Leads to the Induction of the Apoptotic Machinery

In the presence of environmental stress, eukaryotic cells can react with specific cellular responses to counteract the impairment of cellular functionality. For example, if this is impossible due to the concentration of exogenous stimuli being too high, cells initiate apoptosis to protect the surrounding tissue. During apoptosis, cell components are degraded in a finely regulated manner, which prevents the release of potentially inflammatory cellular factors to the ambient tissue [20].

NIPP-induced stress triggered the induction of apoptosis in the tumor cells. The increased activity of apoptotic effector caspases 3 and 7 (Casp-3/7 assay) and apoptosis-specific degradation of genomic DNA (TUNEL assay) were detected in MCF-7 cells 24, 48, and 72 h after 20 s of NIPP treatment (Figure 7a). These significant effects could be confirmed in MDA-MB-231 cells (Figure 7b). Evaluation of the non-normalized apoptotic signals per cell demonstrated that the values obtained with both assays were between the non-labeled negative controls and the experimentally induced positive controls (Table 1). However, the clearly higher apoptotic signature of the control approaches compared with the negative controls also indicated an artificially higher apoptotic background.

These results at the level of the apoptotic cell response could be confirmed at the molecular level of gene expression. Both the mRNA of the pro-apoptotic regulator Bcl-2 antagonist of cell death (BAD) and the initiator caspase-9 (Casp-9) were upregulated 48 h after NIPP treatment in both cancer cell lines (Figure 7c,d). After 120 s of treatment, the NIPP-induced devitalizing effect was so pronounced that the target mRNAs were no longer detectable in each replicate.

Figure 7. Apoptosis assays. The breast cancer cells MCF-7 (**a**) and MDA-MB-231 (**b**) were treated with non-invasive physical plasma (NIPP) for 20 s and incubated for an additional 24, 48, and 72 h. Subsequently, caspase-3/7 (Casp-3/7) and terminal deoxynucleotidyl transferase dUTP nick end labeling (TUNEL) apoptosis assays were performed. Casp-3/7 was performed using CellEvent™ Caspase-3/7 Green Detection Reagent and TUNEL assay was performed using TiterTACS in situ apoptosis detection kit. Fluorescence signals were detected at 535 nm (Casp-3/7 assay) and 450 nm (TUNEL assay) in an Infinite M200 Pro microplate reader. In another approach, the two pro-apoptotic factors Bcl-2 antagonist of cell death (BAD) and caspase-9 (Casp-9) were detected in MCF-7 (**c**) and MDA-MB-231 (**d**) cells by quantitative reverse transcription-polymerase chain reaction (qRT-PCR). Analyses were performed 48 h after NIPP treatment of 20, 60, and 120 s applying target-specific primer pairs. Apoptotic values were expressed as relative signals normalized to controls. The results are displayed as mean $\pm$ standard deviation ($p \leq 0.05$ *; $p \leq 0.01$ **; $p \leq 0.001$ ***).

Table 1. Absolute representation of apoptosis. As shown in Figure 7a,b, the breast cancer cells MCF-7 and MDA-MB-231 were treated with NIPP for 20 s and incubated for an additional 24, 48, and 72 h. Subsequently, caspase-3/-7 (Casp-3/7) and terminal deoxynucleotidyl transferase dUTP nick end labeling TUNEL apoptosis assays were performed. To illustrate the absolute apoptotic events, the measured values (apoptotic signals/cell) are shown without normalization of NIPP treatment to controls. Additionally shown are negative controls (Neg Ctrl) and positive controls (Pos Ctrl) for both assays in both cell lines. The results are displayed as mean ± standard deviation.

Cells	Assay	Neg Ctrl	Pos Ctrl	Ctrl			NIPP		
				24 h	48 h	72 h	24 h	48 h	72 h
MCF-7	Casp-3/7	1.5×10^{-1} $\pm 9.8 \times 10^{-2}$	2.1×10^{0} $\pm 3.2 \times 10^{-1}$	1.9×10^{-1} $\pm 1.2 \times 10^{-2}$	2.5×10^{-1} $\pm 4.2 \times 10^{-2}$	2.6×10^{-1} $\pm 1.7 \times 10^{-1}$	4.4×10^{-1} $\pm 4.6 \times 10^{-2}$	5.9×10^{-1} $\pm 1.4 \times 10^{-1}$	5.9×10^{-1} $\pm 3.5 \times 10^{-1}$
	TUNEL	1.5×10^{-5} $\pm 1.0 \times 10^{-5}$	8.4×10^{-5} $\pm 8.8 \times 10^{-5}$	8.2×10^{-6} $\pm 2.6 \times 10^{-6}$	9.6×10^{-6} $\pm 6.2 \times 10^{-6}$	1.9×10^{-5} $\pm 6.3 \times 10^{-6}$	1.7×10^{-5} $\pm 4.2 \times 10^{-6}$	2.2×10^{-5} $\pm 8.6 \times 10^{-6}$	3.2×10^{-5} $\pm 9.9 \times 10^{-6}$
MDA-MB-231	Casp-3/7	8.3×10^{-2} $\pm 5.2 \times 10^{-2}$	1.4×10^{0} $\pm 6.8 \times 10^{-1}$	2.8×10^{-1} $\pm 9.4 \times 10^{-2}$	3.2×10^{-1} $\pm 1.3 \times 10^{-1}$	2.3×10^{-1} $\pm 5.6 \times 10^{-2}$	5.7×10^{-1} $\pm 1.3 \times 10^{-1}$	9.7×10^{-1} $\pm 3.9 \times 10^{-1}$	6.1×10^{-1} $\pm 1.0 \times 10^{-1}$
	TUNEL	1.9×10^{-6} $\pm 1.2 \times 10^{-6}$	2.3×10^{-5} $\pm 2.5 \times 10^{-5}$	4.1×10^{-6} $\pm 1.6 \times 10^{-6}$	4.3×10^{-6} $\pm 2.2 \times 10^{-6}$	5.4×10^{-6} $\pm 7.5 \times 10^{-7}$	6.1×10^{-6} $\pm 2.7 \times 10^{-6}$	1.1×10^{-5} $\pm 3.7 \times 10^{-6}$	1.0×10^{-5} $\pm 3.5 \times 10^{-6}$

3.6. NIPP Efficacy on Cancer Cells Leads to Reduced Cell Growth

Apoptosis in a subset of cancer cells inactivates these cells and eliminates them from the cell population. Among other potential mechanisms, this apoptotic event should reduce the cell number compared to control cells, leading to reduced growth kinetics overall [21]. Therefore, cancer cells were treated once for 20 s with NIPP and cell growth was monitored for 120 h.

Growth kinetics of both cancer cell lines demonstrated a statistically significant reduction in cell number from 48 h (MCF-7; Figure 8a) and from 24 h (MDA-MB-231; Figure 8b) after NIPP treatment, respectively. The argon-treated control cells showed a nearly exponential growth curve over the entire incubation time. In contrast, the number of live NIPP-treated cells increased only marginally above the initial cell numbers seeded in these growth experiments (MCF-7: 4.5×10^4 cells/well; MDA-MB-231: 3.0×10^4 cells/well).
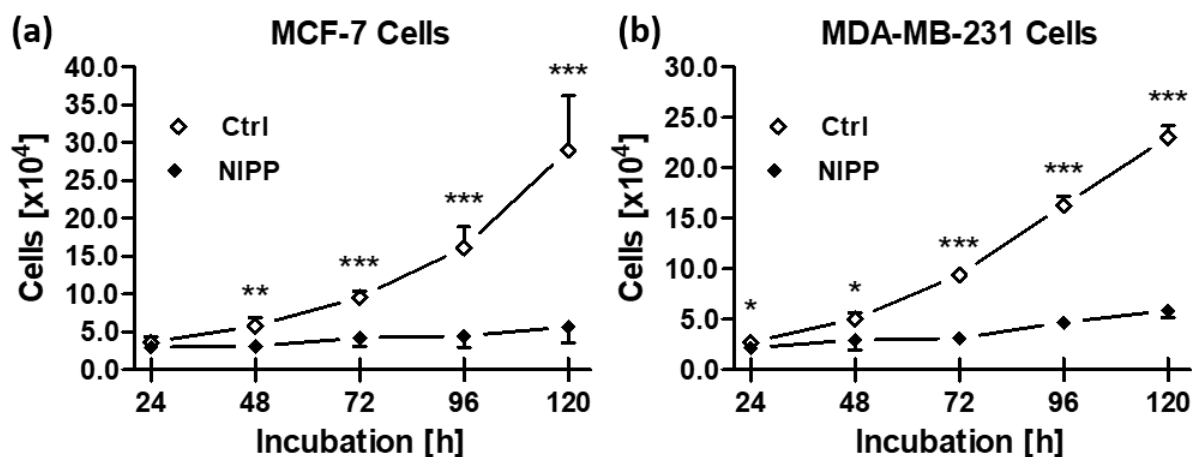
Figure 8. Cell growth assay. Breast cancer cells MCF-7 (**a**) and MDA-MB-231 (**b**) were treated with NIPP for 20 s, incubated for 120 h at 37 °C and 5% CO_2, and live-cell numbers were determined at the indicated time points (CASY Cell Counter and Analyzer model TT). The results are displayed as mean ± standard deviation ($p \leq 0.05$ *; $p \leq 0.01$ **; $p \leq 0.001$ ***).

4. Discussion

While NIPP-induced damage to bacterial cell membranes has been extensively studied [22,23], the impact of NIPP on the cytoplasmic membrane of eukaryotic cells, particularly the effects on permeability to low molecular weight compounds, is poorly investigated. Recent studies have demonstrated increased cytoplasmic membrane permeability after NIPP treatment of skeletal sarcoma cells [6,24,25] and NIPP-induced changes in the

membrane potential of keratinocytes [26]. Moreover, characterization by Raman imaging identified significant alteration of the molecular fingerprint of phospholipids following NIPP treatment with different plasma devices [27]. The present study revealed that low molecular weight compounds ($\leq$10 kDa) could pass unimpaired through the cytoplasmic membrane of breast cancer cells after NIPP treatment. This effect on the molecule passing seems dose-independent as NIPP treatment times of 20 and 60 s demonstrated no dose-dependent variation on permeability. Changes in membrane integrity after NIPP treatment has been previously reported in osteosarcoma cells [25]. FDA efflux could be shown in osteosarcoma cells after NIPP treatment in a concentration-dependent manner. The discrepancy between the sensitivity to different NIPP concentrations indicates a possible tumor entity-specific NIPP efficiency.

The release of small molecules such as those of ATP has been associated with NIPP-induced damage-associated molecular patterns, enhancing cellular visibility to the immune system [28]. In this study, NIPP treatment resulted in an efflux of endogenously synthesized ATP, ruling out artificial and toxic effects of the fluorescent dye incubation. This ATP release was also demonstrated in malignant cells of the skin and the pancreas [29]. Although ATP can also be liberated from apoptotic cells and induce macrophage activation [30,31], apoptosis-induced ATP release can be excluded in the present study. NIPP-induced ATP efflux could be detected immediately after cancer cell treatment. However, NIPP-induced apoptosis would not occur until many hours after treatment, so even early apoptotic processes cannot be responsible for ATP release [32]. In contrast to the incubation experiments with fluorescent dyes, NIPP-induced ATP release exhibited a clear positive correlation with treatment duration. Whether the chemical structure of the released molecules plays a role in the accelerated transfer through the cytoplasmic membrane or whether the incubation with dyes can lead to artificial effects cannot be ruled out at this point.

One explanation for the enhanced extracellular ATP concentration could be the increased cell permeability mediated by NIPP-induced ROS including H_2O_2 [33].

ROS are the primary mediators of the effects of NIPP on cancer cells [34–37], and their formation depends on carrier gas flow rate and treatment duration. Endogenously, ROS are formed in physiologically highly active and fast-growing cancer cells, mostly during oxidative ATP synthesis, but can be neutralized by cellular detoxification systems [38,39]. NIPP generated ROS lead to higher ROS concentrations into cancer cells and overcome the capacity of the biochemical detoxification machinery. Therefore, NIPP-induced ROS can damage the cytoplasmic membrane and intracellular membrane compartments such as the nuclear membrane, the endoplasmic reticulum, and the mitochondria. The exact mechanism of NIPP-induced ROS on membranes is not yet fully understood [40]. However, the ROS-mediated damage to mitochondrial functionality after NIPP treatment has already been demonstrated [41]. Therefore, in addition to the observed decrease in ATP levels, cellular ATP biosynthesis in mitochondria would also be impeded. Restrictions in cancer cell energy metabolism and severe disruption of energy metabolism by NIPP treatment induce apoptosis and diminish proliferation [41], as shown in this study at the cellular and molecular level (Figure 9). This observation goes in line with other studies, showing that sustained cellular (redox) stress leads to adaptations in gene expression in breast cancer cells at the level of DNA methylation [42,43] and apoptotic and proliferative signaling cascades [39]. These NIPP effects were demonstrated in both malignant and non-malignant human breast cells [35,44,45]. However, our study also showed that some apoptotic background is already induced during the experimental handling of the control approaches. It is unknown by what means these secondary effects are triggered (e.g., separation and seeding of the cells, temperature variations, mechanical stress). On the other hand, it should be noted that, compared with these artificial effects, NIPP treatment also induces significantly higher apoptosic rates.

The biochemical activity of ROS both as oxidizing agents as well as cellular signaling molecules can explain a higher sensitivity of cancer cells to NIPP treatment. As mentioned above, NIPP application leads to a significant increase in ROS concentrations, which in turn

cannot be neutralized efficiently by the cellular detoxification systems of physiologically highly active cancer cells. However, since adjacent non-malignant cells of the tissue still have a significantly higher detoxification capacity, they are affected considerably less or even not at all by NIPP treatment [5]. This hypothesis may account for a cancer-specific efficacy of NIPP in terms of a significantly higher sensitivity compared to physiologically healthy cells. On the other hand, this phenomenon explains the frequently observed good tolerability of NIPP in clinical use. So far, no significant side effects of NIPP treatment have been described [46], which is of great relevance for the use of NIPP, especially in otherwise very invasive and cytotoxic therapies of neoplasia.
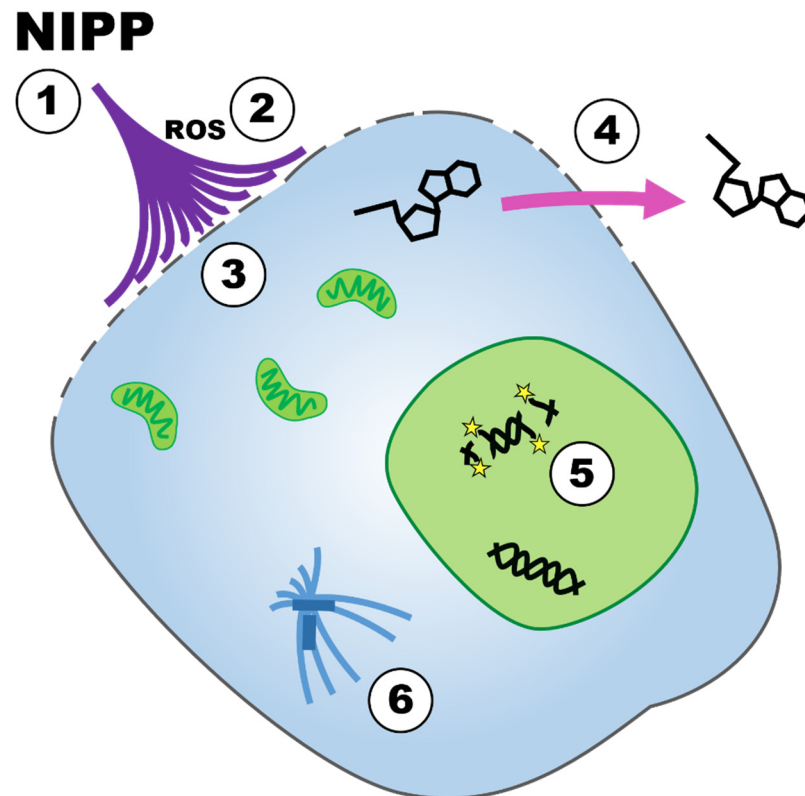
Figure 9. Model for the devitalizing NIPP efficacy on tumor cells. NIPP treatment of tumor cells (1) leads to the formation of ROS (2), which interfere with the cytoplasmic membrane and increase its permeability (3). Subsequently, the loss of ATP leads to the impairment of cellular metabolism (4), which induces apoptosis in part of the cell population (5) and reduces the growth of the entire cell population (6).

Recent in vitro data, including the present study, suggest promising clinical applications of NIPP in gynecology [47–50]. The local effect of NIPP makes its use in combination with established procedures especially promising. The broad spectrum of mechanisms of action and thus of therapeutic targets could potentially also lead to increased therapeutic efficiency. In addition, there is the option of using NIPP-treated liquids for therapy. In this application, very comparable effects to direct NIPP treatment of cancer cells have been demonstrated in vitro [7,51].

Furthermore, a combination of NIPP treatment and chemotherapy rinsing (hyperthermic intraperitoneal chemotherapy, HIPEC; pressurized intraperitoneal aerosol chemotherapy, PIPAC) would be feasible. The enhanced permeability of the cytoplasmic membrane may enhance drug delivery into cancer cells. This could lead to a mitigation of the dose and thus to a reduction in the undesirable side effects of the drug [52–54].

In summary, the anticancer effect of NIPP can be attributed to a significant extent to the functional restriction of the cytoplasmic membrane of cancer cells. The resulting

impairment of cell physiology leads to apoptosis of a subset of cancer cells and reduced cell growth of the remaining part of the cancer cell population. This effect opens up a wide range of applications in oncological therapy and the treatment of non-malignant precancerous lesions.

References

1. Kletschkus, K.; Haralambiev, L.; Mustea, A.; Bekeschus, S.; Stope, M.B. Review of innovative physical therapy methods: Introduction to the principles of cold physical plasma. *In Vivo* **2020**, *34*, 3103–3107. [CrossRef]
2. Gan, L.; Jiang, J.; Duan, J.W.; Wu, X.J.Z.; Zhang, S.; Duan, X.R.; Song, J.Q.; Chen, H.X. Cold atmospheric plasma applications in dermatology: A systematic review. *J. Biophotonics* **2021**, *14*, e202000415. [CrossRef] [PubMed]
3. Gan, L.; Zhang, S.; Poorun, D.; Liu, D.; Lu, X.; He, M.; Duan, X.; Chen, H. Medical applications of nonthermal atmospheric pressure plasma in dermatology. *J. Dtsch. Dermatol. Ges.* **2018**, *16*, 7–13. [CrossRef] [PubMed]
4. Yan, D.; Sherman, J.H.; Keidar, M. Cold atmospheric plasma, a novel promising anti-cancer treatment modality. *Oncotarget* **2017**, *8*, 15977–15995. [CrossRef] [PubMed]
5. Stope, M.B. Plasma oncology—Physical plasma as innovative tumor therapy. *J. Cancer Biol.* **2020**, *1*, 53–56. [CrossRef]
6. Jacoby, J.M.; Strakeljahn, S.; Nitsch, A.; Bekeschus, S.; Hinz, P.; Mustea, A.; Ekkernkamp, A.; Tzvetkov, M.V.; Haralambiev, L.; Stope, M.B. An innovative therapeutic option for the treatment of skeletal sarcomas: Elimination of osteo- and Ewing's sarcoma cells using physical gas plasma. *Int. J. Mol. Sci.* **2020**, *21*, 4460. [CrossRef]
7. Koensgen, D.; Besic, I.; Gümbel, D.; Kaul, A.; Weiss, M.; Diesing, K.; Kramer, A.; Bekeschus, S.; Mustea, A.; Stope, M.B. Cold atmospheric plasma (CAP) and CAP-stimulated cell culture media suppress ovarian cancer cell growth—A putative treatment option in ovarian cancer therapy. *Anticancer Res.* **2017**, *37*, 6739–6744. [CrossRef]
8. Weiss, M.; Gümbel, D.; Hanschmann, E.-M.; Mandelkow, R.; Gelbrich, N.; Zimmermann, U.; Walther, R.; Ekkernkamp, A.; Sckell, A.; Kramer, A.; et al. Cold atmospheric plasma treatment induces anti-proliferative effects in prostate cancer cells by redox and apoptotic signaling pathways. *PLoS ONE* **2015**, *10*, e0130350. [CrossRef]
9. van Loenhout, J.; Flieswasser, T.; Freire Boullosa, L.; de Waele, J.; van Audenaerde, J.; Marcq, E.; Jacobs, J.; Lin, A.; Lion, E.; Dewitte, H.; et al. Cold atmospheric plasma-treated PBS eliminates immunosuppressive pancreatic Stellate cells and induces immunogenic cell death of pancreatic cancer cells. *Cancers* **2019**, *11*, 597. [CrossRef]
10. Kim, J.Y.; Ballato, J.; Foy, P.; Hawkins, T.; Wei, Y.; Li, J.; Kim, S.-O. Apoptosis of lung carcinoma cells induced by a flexible optical fiber-based cold microplasma. *Biosens. Bioelectron.* **2011**, *28*, 333–338. [CrossRef]
11. Hediger, M.A.; Clémençon, B.; Burrier, R.E.; Bruford, E.A. The ABCs of membrane transporters in health and disease (SLC series): Introduction. *Mol. Asp. Med.* **2013**, *34*, 95–107. [CrossRef] [PubMed]
12. Yang, N.J.; Hinner, M.J. Getting across the cell membrane: An overview for small molecules, peptides, and proteins. *Methods Mol. Biol.* **2015**, *1266*, 29–53. [CrossRef] [PubMed]
13. Striesow, J.; Lackmann, J.-W.; Ni, Z.; Wenske, S.; Weltmann, K.-D.; Fedorova, M.; Woedtke, T.; von Wende, K. Oxidative modification of skin lipids by cold atmospheric plasma (CAP): A standardizable approach using RP-LC/MS(2) and DI-ESI/MS(2). *Chem. Phys. Lipids* **2020**, *226*, 104786. [CrossRef]
14. Guo, L.; Zhao, Y.; Liu, D.; Liu, Z.; Chen, C.; Xu, R.; Tian, M.; Wang, X.; Chen, H.; Kong, M.G. Cold atmospheric-pressure plasma induces DNA-protein crosslinks through protein oxidation. *Free Radic. Res.* **2018**, *52*, 783–798. [CrossRef]
15. Sung, H.; Ferlay, J.; Siegel, R.L.; Laversanne, M.; Soerjomataram, I.; Jemal, A.; Bray, F. Global cancer statistics 2020: GLOBOCAN estimates of incidence and mortality worldwide for 36 cancers in 185 countries. *CA Cancer J. Clin.* **2021**, *71*, 209–249. [CrossRef]
16. Fisusi, F.A.; Akala, E.O. Drug combinations in breast cancer therapy. *Pharm. Nanotechnol.* **2019**, *7*, 3–23. [CrossRef]
17. Ravandeh, M.; Kahlert, H.; Jablonowski, H.; Lackmann, J.-W.; Striesow, J.; Agmo Hernández, V.; Wende, K. A combination of electrochemistry and mass spectrometry to monitor the interaction of reactive species with supported lipid bilayers. *Sci. Rep.* **2020**, *10*, 18683. [CrossRef] [PubMed]

18. Bourke, P.; Ziuzina, D.; Han, L.; Cullen, P.J.; Gilmore, B.F. Microbiological interactions with cold plasma. *J. Appl. Microbiol.* **2017**, *123*, 308–324. [CrossRef]

19. Nitsch, A.; Haralambiev, L.; Einenkel, R.; Muzzio, D.O.; Zygmunt, M.T.; Ekkernkamp, A.; Burchardt, M.; Stope, M.B. Determination of in vitro membrane permeability by analysis of intracellular and extracellular fluorescein signals in renal cells. *In Vivo* **2019**, *33*, 1767–1771. [CrossRef]

20. Miyata, Y.; Matsuo, T.; Sagara, Y.; Ohba, K.; Ohyama, K.; Sakai, H. A Mini-review of reactive oxygen species in urological cancer: Correlation with NADPH oxidases, angiogenesis, and apoptosis. *Int. J. Mol. Sci.* **2017**, *18*, 2214. [CrossRef]

21. Haralambiev, L.; Bandyophadyay, A.; Suchy, B.; Weiss, M.; Kramer, A.; Bekeschus, S.; Ekkernkamp, A.; Mustea, A.; Kaderali, L.; Stope, M.B. Determination of Immediate vs. Kinetic growth retardation in physically plasma-treated cells by experimental and modelling data. *Anticancer Res.* **2020**, *40*, 3743–3749. [CrossRef]

22. Dolphin, C.T.; Caldwell, J.; Smith, R.L. Depression of oxidative metabolism of aspirin in mice via an interferon-associated mechanism in relation to Reye's syndrome. *J. Pharm. Pharmacol.* **1987**, *39*, 228–230. [CrossRef] [PubMed]

23. Yu, Q.S.; Huang, C.; Hsieh, F.-H.; Huff, H.; Duan, Y. Bacterial inactivation using a low-temperature atmospheric plasma brush sustained with argon gas. *J. Biomed. Mater. Res. B Appl. Biomater.* **2007**, *80*, 211–219. [CrossRef]

24. Haralambiev, L.; Nitsch, A.; Jacoby, J.M.; Strakeljahn, S.; Bekeschus, S.; Mustea, A.; Ekkernkamp, A.; Stope, M.B. Cold atmospheric plasma treatment of chondrosarcoma cells affects proliferation and cell membrane permeability. *Int. J. Mol. Sci.* **2020**, *21*, 2291. [CrossRef]

25. Haralambiev, L.; Nitsch, A.; Einenkel, R.; Muzzio, D.O.; Gelbrich, N.; Burchardt, M.; Zygmunt, M.; Ekkernkamp, A.; Stope, M.B.; Gümbel, D. The effect of cold atmospheric plasma on the membrane permeability of human osteosarcoma cells. *Anticancer Res.* **2020**, *40*, 841–846. [CrossRef]

26. Dezest, M.; Chavatte, L.; Bourdens, M.; Quinton, D.; Camus, M.; Garrigues, L.; Descargues, P.; Arbault, S.; Burlet-Schiltz, O.; Casteilla, L.; et al. Mechanistic insights into the impact of cold atmospheric pressure plasma on human epithelial cell lines. *Sci. Rep.* **2017**, *7*, 41163. [CrossRef] [PubMed]

27. Wenzel, T.; Carvajal Berrio, D.A.; Daum, R.; Reisenauer, C.; Weltmann, K.D.; Wallwiener, D.; Brucker, S.Y.; Schenke-Layland, K.; Brauchle, E.M.; Weiss, M. Molecular effects and tissue penetration depth of physical plasma in human mucosa analyzed by contact- and marker-independent Raman microspectroscopy. *ACS Appl. Mater. Interfaces* **2019**, *11*, 42885–42895. [CrossRef] [PubMed]

28. Miller, V.; Lin, A.; Fridman, A. Why target immune cells for plasma treatment of cancer. *Plasma Chem. Plasma Process* **2016**, *36*, 259–268. [CrossRef]

29. Azzariti, A.; Iacobazzi, R.M.; Di Fonte, R.; Porcelli, L.; Gristina, R.; Favia, P.; Fracassi, F.; Trizio, I.; Silvestris, N.; Guida, G.; et al. Plasma-activated medium triggers cell death and the presentation of immune activating danger signals in melanoma and pancreatic cancer cells. *Sci. Rep.* **2019**, *9*, 4099. [CrossRef]

30. Kepp, O.; Senovilla, L.; Vitale, I.; Vacchelli, E.; Adjemian, S.; Agostinis, P.; Apetoh, L.; Aranda, F.; Barnaba, V.; Bloy, N.; et al. Consensus guidelines for the detection of immunogenic cell death. *Oncoimmunology* **2014**, *3*, 955691. [CrossRef]

31. Lin, A.; Truong, B.; Patel, S.; Kaushik, N.; Choi, E.H.; Fridman, G.; Fridman, A.; Miller, V. Nanosecond-pulsed DBD plasma-generated reactive oxygen species trigger immunogenic cell death in A549 lung carcinoma cells through intracellular oxidative stress. *Int. J. Mol. Sci.* **2017**, *18*, 966. [CrossRef] [PubMed]

32. Elliott, M.R.; Chekeni, F.B.; Trampont, P.C.; Lazarowski, E.R.; Kadl, A.; Walk, S.F.; Park, D.; Woodson, R.L.; Ostankovich, M.; Sharma, P.; et al. Nucleotides released by apoptotic cells act as a find-me signal to promote phagocytic clearance. *Nature* **2009**, *461*, 282–286. [CrossRef] [PubMed]

33. Xu, D.; Wang, B.; Xu, Y.; Chen, Z.; Cui, Q.; Yang, Y.; Chen, H.; Kong, M.G. Intracellular ROS mediates gas plasma-facilitated cellular transfection in 2D and 3D cultures. *Sci. Rep.* **2016**, *6*, 27872. [CrossRef]

34. Lu, X.; Naidis, G.V.; Laroussi, M.; Reuter, S.; Graves, D.B.; Ostrikov, K. Reactive species in non-equilibrium atmospheric-pressure plasmas: Generation, transport, and biological effects. *Phys. Rep.* **2016**, *630*, 1–84. [CrossRef]

35. Nguyen, N.H.; Park, H.J.; Yang, S.S.; Choi, K.S.; Lee, J.-S. Anti-cancer efficacy of nonthermal plasma dissolved in a liquid, liquid plasma in heterogeneous cancer cells. *Sci. Rep.* **2016**, *6*, 29020. [CrossRef]

36. Chen, Z.; Zhang, S.; Levchenko, I.; Beilis, I.I.; Keidar, M. In vitro demonstration of cancer inhibiting properties from stratified self-organized plasma-liquid interface. *Sci. Rep.* **2017**, *7*, 12163. [CrossRef]

37. Ninomiya, K.; Ishijima, T.; Imamura, M.; Yamahara, T.; Enomoto, H.; Takahashi, K.; Tanaka, Y.; Uesugi, Y.; Shimizu, N. Evaluation of extra- and intracellular OH radical generation, cancer cell injury, and apoptosis induced by a non-thermal atmospheric-pressure plasma jet. *J. Phys. D Appl. Phys.* **2013**, *46*, 425401. [CrossRef]

38. Mitra, S.; Nguyen, L.N.; Akter, M.; Park, G.; Choi, E.H.; Kaushik, N.K. Impact of ROS generated by chemical, physical, and llasma techniques on cancer attenuation. *Cancers* **2019**, *11*, 1030. [CrossRef]

39. Ott, M.; Gogvadze, V.; Orrenius, S.; Zhivotovsky, B. Mitochondria, oxidative stress and cell death. *Apoptosis* **2007**, *12*, 913–922. [CrossRef]

40. Lin, L.; Ding, C.B.; Jin, T.; Han, X.H.; Zhou, H.; Wu, Z.W.; Pan, Y.Y. A meaningful attempt: Applying dielectric barrier discharge plasma to induce apoptosis of MDA-MB-231 cells via regulating HIF-1α/VEGFA expression. *Surf. Coat. Technol.* **2020**, *41*, 126293. [CrossRef]

41. Adachi, T.; Tanaka, H.; Nonomura, S.; Hara, H.; Kondo, S.-I.; Hori, M. Plasma-activated medium induces A549 cell injury via a spiral apoptotic cascade involving the mitochondrial-nuclear network. *Free Radic. Biol. Med.* **2015**, *79*, 28–44. [CrossRef] [PubMed]

42. Lee, S.; Lee, H.; Bae, H.; Choi, E.H.; Kim, S.J. Epigenetic silencing of miR-19a-3p by cold atmospheric plasma contributes to proliferation inhibition of the MCF-7 breast cancer cell. *Sci. Rep.* **2016**, *6*, 30005. [CrossRef] [PubMed]

43. Park, S.B.; Kim, B.; Bae, H.; Lee, H.; Lee, S.; Choi, E.H.; Kim, S.J. Differential epigenetic effects of atmospheric cold plasma on MCF-7 and MDA-MB-231 breast cancer cells. *PLoS ONE* **2015**, *10*, e0129931. [CrossRef] [PubMed]

44. Kalghatgi, S.; Kelly, C.M.; Cerchar, E.; Torabi, B.; Alekseev, O.; Fridman, A.; Friedman, G.; Azizkhan-Clifford, J. Effects of non-thermal plasma on mammalian cells. *PLoS ONE* **2011**, *6*, e16270. [CrossRef]

45. Kalghatgi, S.; Fridman, A.; Azizkhan-Clifford, J.; Friedman, G. DNA damage in mammalian cells by non-thermal atmospheric pressure microsecond pulsed dielectric barrier discharge plasma is not mediated by ozone. *Plasma Process. Polym.* **2012**, *9*, 726–732. [CrossRef]

46. Schuster, M.; Rutkowski, R.; Hauschild, A.; Shojaei, R.K.; Woedtke, T.; Rana, A.; Bauer, G.; Metelmann, P.; Seebauer, C. Side effects in cold plasma treatment of advanced oral cancer—Clinical data and biological interpretation. *Clin Plasma Med.* **2018**, *10*, 9–15. [CrossRef]

47. Weiss, M.; Stope, M.B. Physical plasma: A new treatment option in gynecological oncology. *Arch. Gynecol. Obstet.* **2018**, *298*, 853–855. [CrossRef]

48. Stope, M.B.; Benouahi, R.; Sander, C.; Haralambiev, L.; Nitsch, A.; Egger, E.; Mustea, A. Protherapeutic effects and inactivation of mammary carcinoma cells by a medical argon plasma device. *Anticancer Res.* **2020**, *40*, 6205–6212. [CrossRef]

49. Wenzel, T.; Carvajal Berrio, D.A.; Reisenauer, C.; Layland, S.; Koch, A.; Wallwiener, D.; Brucker, S.Y.; Schenke-Layland, K.; Brauchle, E.-M.; Weiss, M. Trans-mucosal efficacy of non-thermal plasma treatment on cervical cancer tissue and human cervix uteri by a next generation electrosurgical argon plasma device. *Cancers* **2020**, *12*, 267. [CrossRef]

50. Feil, L.; Koch, A.; Utz, R.; Ackermann, M.; Barz, J.; Stope, M.; Krämer, B.; Wallwiener, D.; Brucker, S.Y.; Weiss, M. Cancer-selective treatment of cancerous and non-cancerous human cervical cell models by a non-thermally operated electrosurgical argon plasma device. *Cancers* **2020**, *12*, 1037. [CrossRef]

51. Tanaka, H.; Mizuno, M.; Ishikawa, K.; Toyokuni, S.; Kajiyama, H.; Kikkawa, F.; Hori, M. New hopes for plasma-based cancer treatment. *Plasma* **2018**, 155. [CrossRef]

52. Sagwal, S.K.; Pasqual-Melo, G.; Bodnar, Y.; Gandhirajan, R.K.; Bekeschus, S. Combination of chemotherapy and physical plasma elicits melanoma cell death via upregulation of SLC22A16. *Cell Death Dis.* **2018**, *9*, 1179. [CrossRef] [PubMed]

53. Daeschlein, G.; Hillmann, A.; Gümbel, D.; Sicher, C.; Podewils, S.; Stope, M.B.; Jünger, M. Enhanced anticancer efficacy by drug chemotherapy and cold atmospheric plasma against melanoma and glioblastoma cell lines in vitro. *IEEE Trans. Radiat. Plasma Med. Sci.* **2018**, *2*, 153–159. [CrossRef]

54. Tempfer, C.B.; Hilal, Z.; Dogan, A.; Petersen, M.; Rezniczek, G.A. Concentrations of cisplatin and doxorubicin in ascites and peritoneal tumor nodules before and after pressurized intraperitoneal aerosol chemotherapy (PIPAC) in patients with peritoneal metastasis. *Eur. J. Surg. Oncol.* **2018**, *44*, 1112–1117. [CrossRef] [PubMed]